



Article

Antibacterial and Sporicidal Activity Evaluation of Theaflavin-3,3'-digallate

Ayuni Yussof, Brian Cammalleri, Oluwanifemi Fayemiwo, Sabrina Lopez and Tinchun Chu *

Department of Biological Sciences, Seton Hall University, South Orange, NJ 07079, USA; mohamesi@shu.edu (A.Y.); cammalbr@shu.edu (B.C.); fayemiol@shu.edu (O.F.); lopezsac@shu.edu (S.L.)
* Correspondence: tinchun.chu@shu.edu

Abstract: Theaflavin-3,3'-digallate (TFDG), a polyphenol derived from the leaves of *Camellia sinensis*, is known to have many health benefits. In this study, the antibacterial effect of TFDG against nine bacteria and the sporicidal activities on spore-forming *Bacillus* spp. have been investigated. Microplate assay, colony-forming unit, BacTiter-Glo™, and Live/Dead Assays showed that 250 µg/mL TFDG was able to inhibit bacterial growth up to 99.97%, while 625 µg/mL TFDG was able to inhibit up to 99.92% of the spores from germinating after a one-hour treatment. Binding analysis revealed the favorable binding affinity of two germination-associated proteins, GPR and Lgt (GerF), to TFDG, ranging from -7.6 to -10.3 kcal/mol. Semi-quantitative RT-PCR showed that TFDG treatment lowered the expression of *gpr*, ranging from 0.20 to 0.39 compared to the control in both *Bacillus* spp. The results suggest that TFDG not only inhibits the growth of vegetative cells but also prevents the germination of bacterial spores. This report indicates that TFDG is a promising broad-spectrum antibacterial and anti-spore agent against Gram-positive, Gram-negative, acid-fast bacteria, and endospores. The potential anti-germination mechanism has also been elucidated.

Keywords: antibacterial; sporicidal; anti-germination; binding analysis; natural product; black tea polyphenol; theaflavin



Citation: Yussof, A.; Cammalleri, B.; Fayemiwo, O.; Lopez, S.; Chu, T. Antibacterial and Sporicidal Activity Evaluation of Theaflavin-3,3'-digallate. *Int. J. Mol. Sci.* **2022**, *23*, 2153. <https://doi.org/10.3390/ijms23042153>

Academic Editor: Helena Felgueiras

Received: 28 December 2021

Accepted: 10 February 2022

Published: 15 February 2022

Publisher's Note: MDPI stays neutral with regard to jurisdictional claims in published maps and institutional affiliations.



Copyright: © 2022 by the authors. Licensee MDPI, Basel, Switzerland. This article is an open access article distributed under the terms and conditions of the Creative Commons Attribution (CC BY) license (<https://creativecommons.org/licenses/by/4.0/>).

1. Introduction

Many medical and scientific journal articles have documented the rising number of antibiotic-resistant bacteria and the multidrug resistance crisis linked to the overuse or abuse of antibiotics [1]. Vancomycin, for example, was first introduced to clinical practice in 1972, and unfortunately, vancomycin-resistant *S. aureus* (VRSA) was reported in 1979 [2]. In the United States, approximately 2.8 million people are infected with antibiotic-resistant bacteria yearly, and at least 35,000 die from the infection [3]. The problem of antibiotic resistance imposes a significant financial burden as evidenced by the number of methicillin-resistant *Staphylococcus aureus* (MRSA)-related issues that cost the US healthcare system around \$3–4 billion annually [4].

The aromatic allure, taste, and health benefits of tea make it one of the most popular beverages worldwide [5]. Both black and green tea are derived from the leaves of *Camellia sinensis* but differ in the level of oxidation due to fermentation [5,6]. Black tea contains a lower level of catechins than green tea but makes up for it with a higher amount of theaflavin [6]. The major theaflavins present in black tea include theaflavin (TF), theaflavin-3-gallate (TF3G), theaflavin-3'-gallate (TF3'G), and theaflavin-3,3'-digallate (TFDG) [6].

Theaflavins (TFs) are the major polyphenols in black tea, showing great potential as an antimicrobial agent. A previous study demonstrated that 1 g of theaflavin mixture extract could contain up to 32.80% of TFDG [7]. As for cellular toxicity, theaflavin has little to no effect on human lung fibroblast tissue, CEM cells, A549, and Vero cells [8]. Compared to epigallocatechin gallate (EGCG), major catechin extracted from green tea, TF is more stable under non-favorable conditions, making it a better candidate for antimicrobial

agents [8]. TFDG was chosen based on a study indicating that TFDG was the most effective in inhibiting *Streptococcus mutans* (*S. mutans*) growth compared to TF, TF3G, and TF3'G [9]. Most previous studies focused on the antioxidant properties of theaflavin. It has been documented that drinking six cups of black tea could significantly increase the antioxidant capacity within the cell [6]. The number of polyphenols in tea varies highly depending on the origin and the brewing technique. Previous studies reported that the level of TFDG ranges from 0.07 to 1.13 g per 100 g of dry leaves among Darjeeling, Assam, Sri Lankan, African, and Chinese tea samples [10]. The level of TFs is approximately 7 mg when brewing a standard US tea bag (2.25 g) in 100 mL of water for less than 2 min and can increase to 14 mg when brewed for more than 4 min [11]. A study using LDL conjugation compared the antioxidant properties of theaflavin to green tea polyphenols, including epicatechin (EC), epicatechin gallate (ECG), epigallocatechin (EGC), and EGCG. The result showed that TFDG > ECG > EGCG \geq TF3'G \geq TF3G > TF \geq EC > EGC in terms of antioxidant properties [12]. Based on the promising results, interest has expanded into the antiviral and antibacterial effects of TFs [8,13–17]. One study indicated 125 $\mu\text{g/mL}$ TFs was the minimum inhibitory concentration (MIC) against *Porphyromonas gingivitis* (*P. gingivalis*) and 250 $\mu\text{g/mL}$ TFDG in *Clostridium perfringens* (*C. perfringens*) while in Hepatitis C virus (HCV), 25 $\mu\text{g/mL}$ TF3 was acting directly on the virus to prevent viral entry into the cell [13,18,19]. Several research groups also investigated the beneficial effect of TFs on the bacterial population and signaling pathways in the oral cavity and gut [20,21]. Some antibacterial mechanisms of TFs have been suggested, including reducing biosynthetic and metabolic activities in *C. perfringens* and anti-hemolytic activity in *Staphylococcus aureus* (*S. aureus*) [13,17].

This study explores the antimicrobial effect against nine pathogenic and clinically significant bacteria. Gram-negative *Klebsiella aerogenes* (*K. aerogenes*) is typically associated with nosocomial outbreaks due to the emergence of multidrug-resistant strains [22]. *Escherichia coli* (*E. coli*), a mutualism in the gastrointestinal (GI) tract of humans, is a model organism for Gram-negative bacteria [23–29]. *Pseudomonas aeruginosa* (*P. aeruginosa*), another nosocomial pathogen found among cystic fibrosis patients with a high mortality rate [30,31], has high resistance to most antimicrobial agents [30]. Multidrug-resistant *Proteus mirabilis* (*P. mirabilis*) is resistant to almost all antibiotic classes, and its prevalence among UTI infections has significantly increased [32].

The “*Bacillus cereus* group” includes several species of closely related pathogenic species like *Bacillus anthracis* (*B. anthracis*) and *Bacillus cereus* (*B. cereus*) [33]. *B. anthracis* and *B. cereus* are the causative agents of anthrax and the emetic syndrome, respectively [33]. *Bacillus subtilis* (*B. subtilis*) is considered a model organism for cellular development, including spore formation, germination, and biofilm production [34,35]. *Bacillus* spores may remain dormant for years but can germinate in favorable conditions such as specific nutrient reintroduction [36–41]. *Staphylococcus aureus* (*S. aureus*) causes a variety of life-threatening diseases, including endocarditis, toxic shock syndrome (TSS), and osteomyelitis [41]. Group A *Streptococcus pyogenes* (*S. pyogenes*) is a beta-hemolytic strain that can cause a wide range of infections, from superficial epithelial infection to the more severe streptococcal TSS (STSS) [42,43].

Acid-fast *Mycobacterium tuberculosis* (*M. tuberculosis*) is the pathogenic bacterium that causes tuberculosis (TB) [44]. Over the past three decades, TB has re-emerged as a global health concern, and in 2019, it is estimated that 10 million people were infected with TB worldwide, and 1.4 million people died [45]. Since detecting multidrug-resistant *M. tuberculosis* (MDR TB), research agencies, non-profit agencies, and academia have spared no effort to develop new treatments [46,47].

This study focuses on the antibacterial and sporicidal activity of TFDG as it contains the highest antioxidant [12] and antiviral [8,19] effects among all theaflavins. Each species used poses a public health threat. Most previous reports centered on the antibacterial activities of green tea polyphenols or a mixture of theaflavins against one or a few species. On the other hand, our results demonstrate that TFDG could potentially serve as a broad-spectrum

antimicrobial agent that can inhibit the growth of nine bacteria across Gram-positive, Gram-negative, and acid-fast groups and an antispore agent. The anti-germination mechanism of TFDG against two *Bacillus* spp. is also proposed. Both 2D and 3D structures of TFDG are displayed in Figure 1. The 3D structure is used for molecular docking analysis.

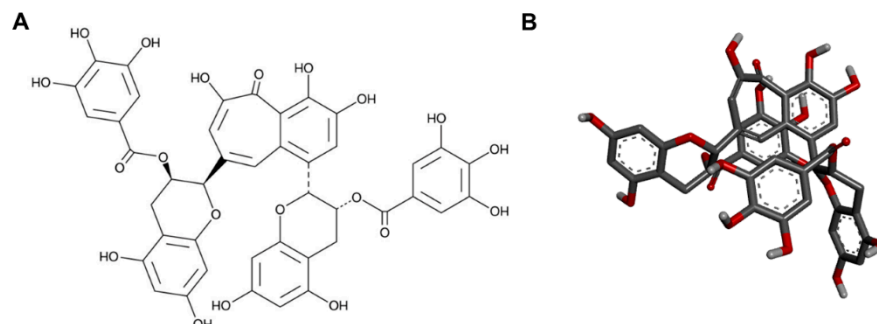


Figure 1. The (A) 2D and (B) 3D chemical structures of TFDG.

2. Results

2.1. Determination of MIC and Half-Maximal Inhibitory Concentration (IC_{50})

No bacterial growth was observed when treated with 250 $\mu\text{g}/\text{mL}$ or higher TFDG, so the MIC was determined as 250 $\mu\text{g}/\text{mL}$. The IC_{50} for all bacteria is around 62.5 $\mu\text{g}/\text{mL}$. As for erythromycin, the IC_{50} ranged from 7 to 26 $\mu\text{g}/\text{mL}$, and the MIC should be greater than 45 $\mu\text{g}/\text{mL}$ for the bacteria tested in this study (Supplementary Figures S1–S3).

2.2. Colony Forming Unit (CFU) Assay

Based on the microplate assay result, the effect of TFDG on the bacteria was further analyzed using CFU assay (Table 1). At the sixth hour, 62.5 $\mu\text{g}/\text{mL}$ was able to inhibit the bacteria from 43.20% to 55.37% and ranged from 93.12% to 99.98% for 250 $\mu\text{g}/\text{mL}$ TFDG. This correlates to the log reduction ranging from 0.25 to 0.35 for 62.5 $\mu\text{g}/\text{mL}$ TFDG and from 1.17 to 3.69 for 250 $\mu\text{g}/\text{mL}$ TFDG. Among nine bacteria tested, 250 $\mu\text{g}/\text{mL}$ TFDG worked the best on *P. aeruginosa* (99.98 \pm 0.01%). All the data were statistically significant ($p < 0.05$).

Table 1. Colony-forming unit (CFU/mL) with the log reduction and percent inhibition of different bacteria with TFDG.

		Bacteria	TFDG ($\mu\text{g/mL}$)	CFU/mL (Mean \pm SD)	Log Reduction (Mean \pm SD)	% Inhibition (Mean \pm SD)	
Gram-negative	<i>K. aerogenes</i>		0	$(9.86 \pm 0.09) \times 10^8$	0	0	
			62.5	$(4.40 \pm 0.12) \times 10^8$	0.35 ± 0.02	$55.37 \pm 1.59\%$	
			250	$(6.07 \pm 0.48) \times 10^7$	1.17 ± 0.03	$93.12 \pm 0.46\%$	
	<i>E. coli</i>		0	$(1.09 \pm 0.06) \times 10^9$	0	0	
			62.5	$(6.20 \pm 0.42) \times 10^8$	0.25 ± 0.01	$43.20 \pm 0.83\%$	
			250	$(2.36 \pm 0.66) \times 10^7$	1.69 ± 0.12	$97.87 \pm 0.52\%$	
	<i>P. aeruginosa</i>		0	$(7.01 \pm 0.07) \times 10^8$	0	0	
			62.5	$(3.68 \pm 0.11) \times 10^8$	0.28 ± 0.01	$47.50 \pm 1.15\%$	
			250	$(1.57 \pm 0.60) \times 10^5$	3.69 ± 0.21	$99.98 \pm 0.01\%$	
	<i>P. mirabilis</i>		0	$(6.27 \pm 0.08) \times 10^9$	0	0	
			62.5	$(3.17 \pm 0.05) \times 10^9$	0.30 ± 0.00	$49.39 \pm 0.23\%$	
			250	$(1.57 \pm 0.39) \times 10^7$	2.62 ± 0.13	$99.75 \pm 0.07\%$	
Gram-positive	Spore former	<i>B. cereus</i>		$(6.54 \pm 0.13) \times 10^8$	0	0	
				62.5	$(3.32 \pm 0.08) \times 10^8$	0.29 ± 0.01	$49.16 \pm 1.65\%$
				250	$(6.00 \pm 1.63) \times 10^5$	3.05 ± 0.13	$99.91 \pm 0.03\%$
		<i>B. subtilis</i>		0	$(6.89 \pm 0.09) \times 10^8$	0	0
				62.5	$(3.35 \pm 0.08) \times 10^8$	0.31 ± 0.01	$51.40 \pm 0.72\%$
				250	$(3.33 \pm 0.82) \times 10^5$	3.34 ± 0.13	$99.95 \pm 0.01\%$
	Non-spore former	<i>S. aureus</i>		0	$(4.69 \pm 0.12) \times 10^9$	0	0
				62.5	$(2.10 \pm 0.18) \times 10^9$	0.35 ± 0.04	$55.20 \pm 4.62\%$
				250	$(3.03 \pm 1.23) \times 10^6$	3.24 ± 0.24	$99.93 \pm 0.03\%$
		<i>S. pyogenes</i>		0	$(4.33 \pm 0.02) \times 10^9$	0	0
				62.5	$(2.24 \pm 0.05) \times 10^9$	0.29 ± 0.01	$48.28 \pm 0.85\%$
				250	$(3.47 \pm 0.09) \times 10^6$	3.10 ± 0.01	$99.92 \pm 0.05\%$
Acid-fast	<i>M. smegmatis</i>		0	$(4.11 \pm 0.07) \times 10^9$	0	0	
			62.5	$(2.02 \pm 0.05) \times 10^9$	0.31 ± 0.02	$50.88 \pm 1.92\%$	
			250	$(1.33 \pm 0.34) \times 10^6$	3.50 ± 0.11	$99.97 \pm 0.01\%$	

2.3. BacTiter-Glo™ Microbial Cell Viability Assay

62.5 $\mu\text{g/mL}$ TFDG was able to inhibit up to $59.82 \pm 6.19\%$ of cell viability based on the ATP level compared to the control, while 250 $\mu\text{g/mL}$ TFDG was able to inhibit up to $99.33 \pm 0.16\%$ of bacteria (Table 2).

Table 2. Relative fluorescence unit (RFU) with the log reduction and percent inhibition of different bacteria treated with TFDG based on BacTiter-Glo™ assay.

		Bacteria	TFDG ($\mu\text{g}/\text{mL}$)	RFU (Mean \pm SD)	Log Reduction (Mean \pm SD)	% Inhibition (Mean \pm SD)	
Gram-negative	<i>K. aerogenes</i>		0	$(1.90 \pm 0.46) \times 10^6$	0	0	
			62.5	$(9.17 \pm 2.01) \times 10^5$	0.31 ± 0.01	$51.52 \pm 1.63\%$	
			250	$(1.51 \pm 0.73) \times 10^4$	2.14 ± 0.12	$99.25 \pm 0.22\%$	
	<i>E. coli</i>		0	$(1.67 \pm 0.09) \times 10^6$	0	0	
			62.5	$(7.89 \pm 1.08) \times 10^5$	0.33 ± 0.04	$53.00 \pm 4.48\%$	
			250	$(1.15 \pm 0.19) \times 10^4$	2.17 ± 0.09	$99.31 \pm 0.14\%$	
	<i>P. aeruginosa</i>		0	$(1.67 \pm 0.36) \times 10^6$	0	0	
			62.5	$(8.07 \pm 1.91) \times 10^5$	0.32 ± 0.02	$51.97 \pm 2.74\%$	
			250	$(6.16 \pm 2.84) \times 10^4$	1.48 ± 0.30	$95.87 \pm 2.39\%$	
	<i>P. mirabilis</i>		0	$(1.52 \pm 0.05) \times 10^6$	0	0	
			62.5	$(7.05 \pm 0.36) \times 10^5$	0.34 ± 0.02	$53.77 \pm 1.69\%$	
			250	$(3.52 \pm 2.45) \times 10^4$	1.78 ± 0.37	$97.71 \pm 1.58\%$	
Gram-positive	Spore former	<i>B. cereus</i>		$(2.03 \pm 1.00) \times 10^6$	0	0	
				62.5	$(7.58 \pm 2.80) \times 10^5$	0.40 ± 0.07	$59.82 \pm 6.19\%$
				250	$(1.28 \pm 0.48) \times 10^5$	1.18 ± 0.08	$93.24 \pm 1.26\%$
		<i>B. subtilis</i>		0	$(2.30 \pm 0.32) \times 10^6$	0	0
				62.5	$(1.09 \pm 0.21) \times 10^5$	0.33 ± 0.03	$52.81 \pm 3.47\%$
				250	$(4.82 \pm 1.41) \times 10^4$	1.69 ± 0.07	$97.94 \pm 0.35\%$
	Non-spore former	<i>S. aureus</i>		$(7.74 \pm 2.02) \times 10^6$	0	0	
				62.5	$(3.66 \pm 1.08) \times 10^6$	0.33 ± 0.03	$53.12 \pm 3.11\%$
				250	$(8.55 \pm 3.73) \times 10^4$	1.98 ± 0.29	$98.71 \pm 0.76\%$
		<i>S. pyogenes</i>		0	$(4.43 \pm 0.99) \times 10^6$	0	0
				62.5	$(2.15 \pm 0.42) \times 10^6$	0.31 ± 0.05	$50.81 \pm 5.81\%$
				250	$(1.01 \pm 0.80) \times 10^5$	1.83 ± 0.50	$97.72 \pm 1.41\%$
Acid-fast	<i>M. smegmatis</i>		0	$(1.83 \pm 0.25) \times 10^6$	0	0	
			62.5	$(9.09 \pm 0.59) \times 10^5$	0.30 ± 0.04	$49.82 \pm 4.42\%$	
			250	$(1.24 \pm 0.42) \times 10^4$	2.19 ± 0.12	$99.33 \pm 0.16\%$	

2.4. Live/Dead Bacterial Viability Assay

Figures 2–4 show the bacterial viability when treated with various concentrations of TFDG after 6 h. Overall, the control bacteria were primarily green and maintained normal morphology. Cells treated with 62.5 $\mu\text{g}/\text{mL}$ TFDG showed a mixture of live, impaired, and dead cells. Most cells appeared to be smaller and more clumped together when compared to the control except for the *M. smegmatis*, which had less aggregation. Cells treated with 250 $\mu\text{g}/\text{mL}$ TFDG were mainly non-viable. The cell numbers were significantly less than the control. The cell morphology appeared smaller and/or segmented with TFDG treatment.

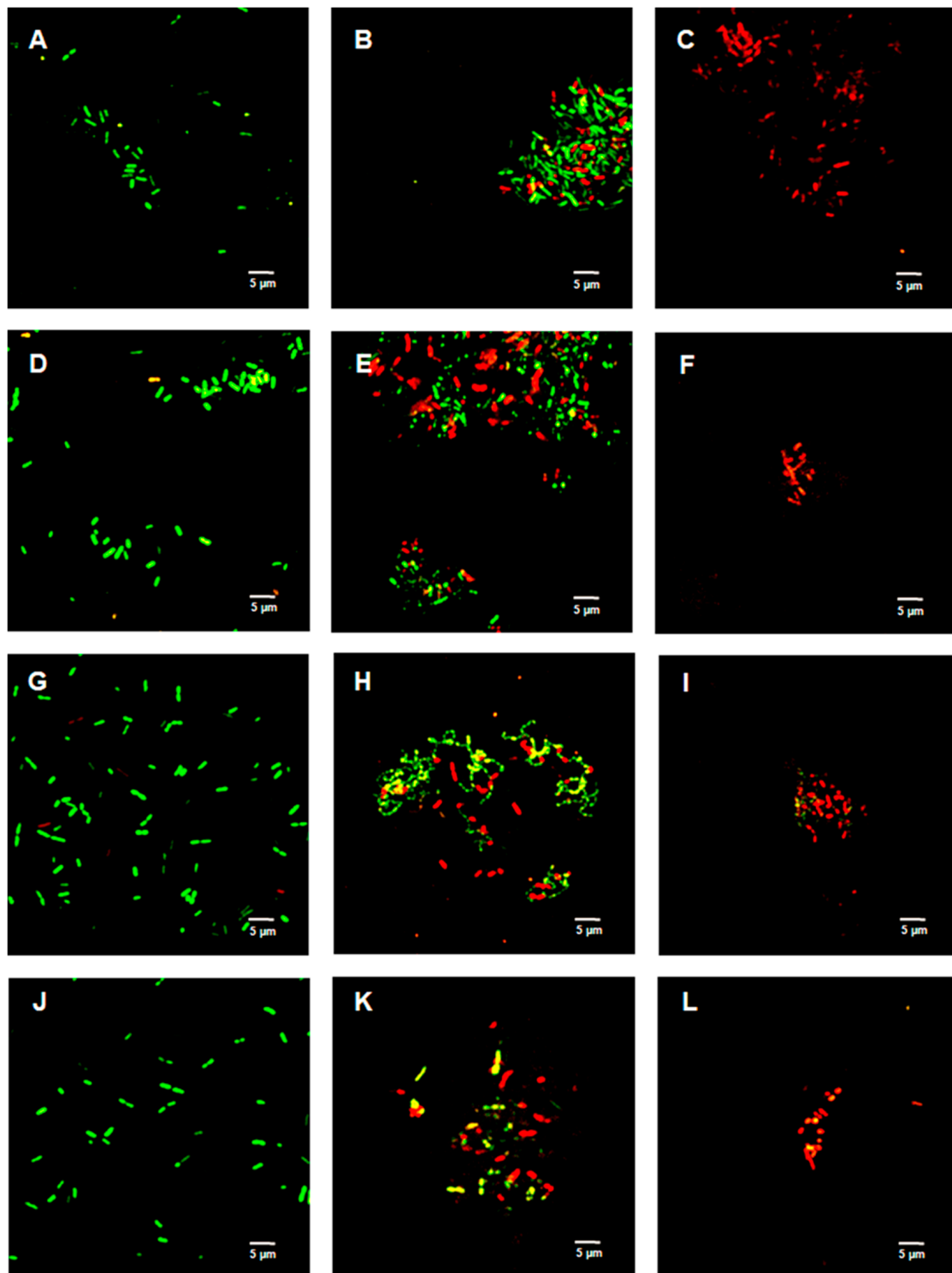


Figure 2. Live/Dead assay of Gram-negative species with various concentrations of TFDG at 6-h incubation. The samples were visualized using Olympus confocal microscope. The green indicates live bacteria, while the red indicates dead bacteria. (A) *K. aerogenes* control; (B) *K. aerogenes* with 62.5 µg/mL TFDG; (C) *K. aerogenes* with 250 µg/mL TFDG; (D) *E. coli* control; (E) *E. coli* with 62.5 µg/mL TFDG; (F) *E. coli* with 250 µg/mL TFDG; (G) *P. aeruginosa* control; (H) *P. aeruginosa* with 62.5 µg/mL TFDG; (I) *P. aeruginosa* with 250 µg/mL TFDG; (J) *P. mirabilis* control; (K) *P. mirabilis* with 62.5 µg/mL TFDG; and (L) *P. mirabilis* with 250 µg/mL TFDG.

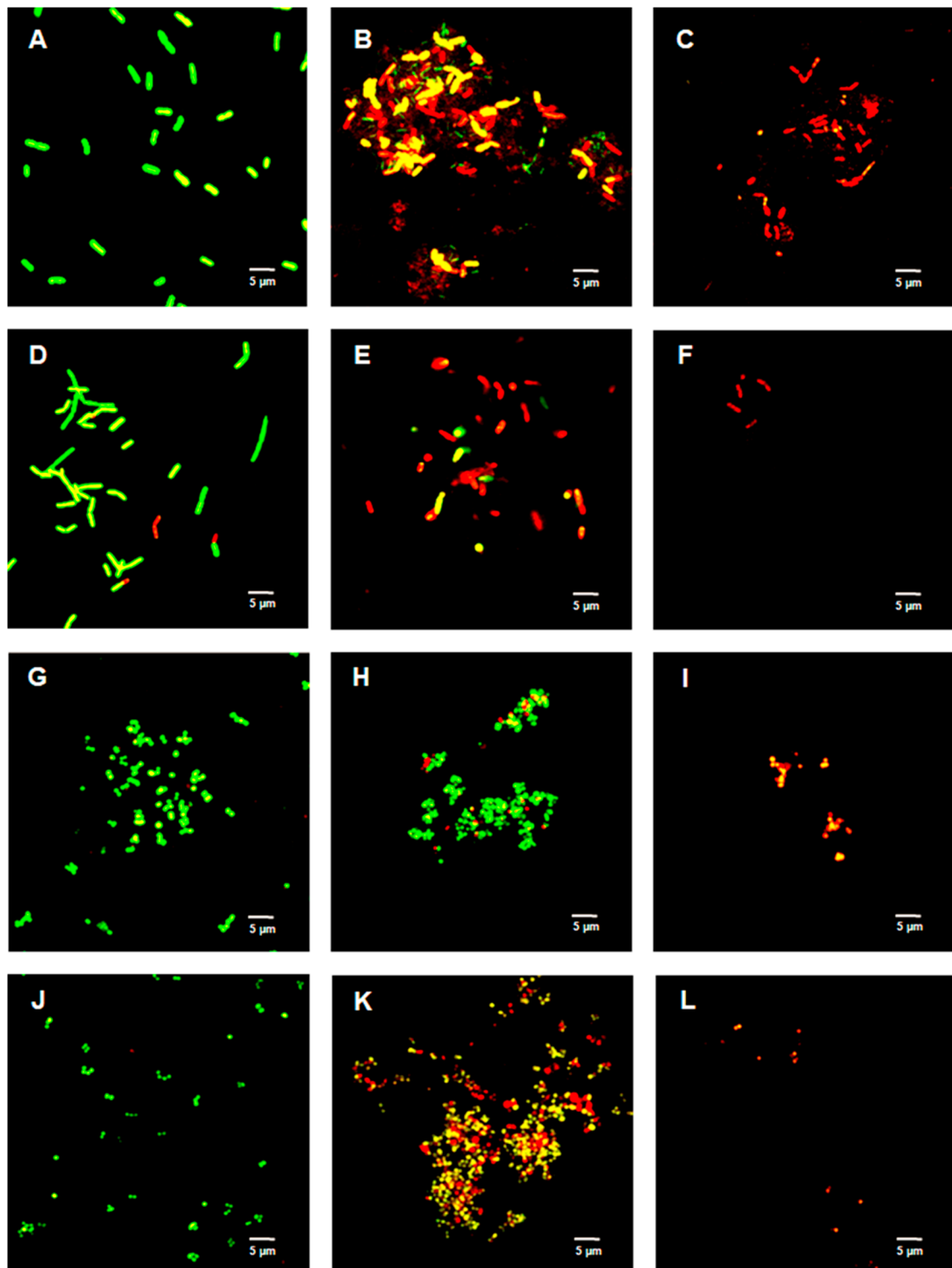


Figure 3. Live/Dead assay of Gram-positive species with various concentrations of TFDG at 6-h incubation. The samples were visualized using Olympus confocal microscope. The green indicates live bacteria, while the red indicates dead bacteria. (A) *B. cereus* control; (B) *B. cereus* with 62.5 µg/mL TFDG; (C) *B. cereus* with 250 µg/mL TFDG; (D) *B. subtilis* control; (E) *B. subtilis* with 62.5 µg/mL TFDG; (F) *B. subtilis* with 250 µg/mL TFDG; (G) *S. aureus* control; (H) *S. aureus* with 62.5 µg/mL TFDG; (I) *S. aureus* with 250 µg/mL TFDG; (J) *S. pyogenes* control; (K) *S. pyogenes* with 62.5 µg/mL TFDG; and (L) *S. pyogenes* with 250 µg/mL TFDG.

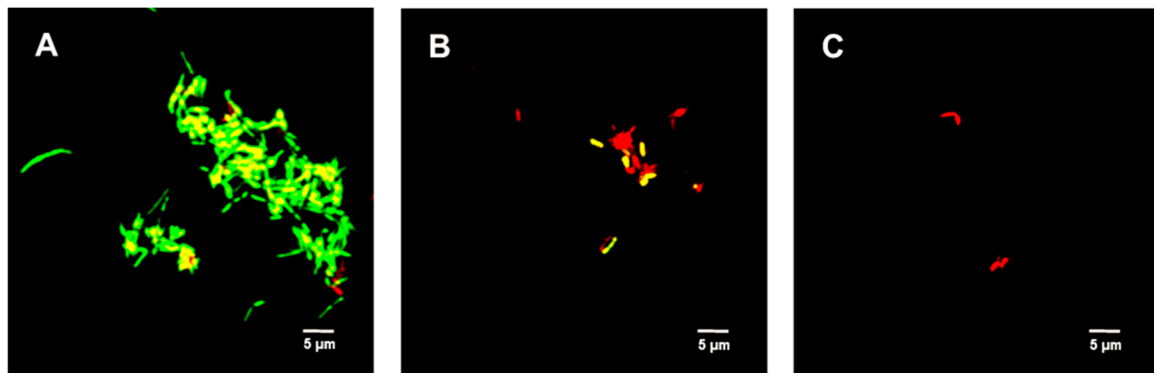


Figure 4. Live/Dead assay of *M. smegmatis* with various concentrations of TFDG at 6-h incubation. The samples were visualized using Olympus confocal microscope. The green indicates live bacteria, while the red indicates dead bacteria. (A) *M. smegmatis* control; (B) *M. smegmatis* with 62.5 µg/mL TFDG; and (C) *M. smegmatis* with 250 µg/mL TFDG.

2.5. Germination Inhibition via CFU Assay

The percent (%) inhibition was calculated from the CFU assay after a 60-min TFDG treatment. 312.5 µg/mL TFDG inhibited the *Bacillus* spores from germinating, ranging from 54.13% to 60.49%, while 625 µg/mL TFDG was able to inhibit germination ranging from 99.37% to 99.92% (Table 3).

Table 3. Germination inhibition assay of both *B. cereus* and *B. subtilis*.

		Bacteria	TFDG (µg/mL)	CFU/mL (Mean ± SD)	Log Reduction (Mean ± SD)	% Inhibition (Mean ± SD)
Gram-positive	Spore former	<i>B. cereus</i>	0	$(1.11 \pm 0.85) \times 10^{10}$	0	0
			312.5	$(4.79 \pm 3.55) \times 10^9$	0.34 ± 0.03	$54.13 \pm 3.51\%$
			625	$(6.55 \pm 4.57) \times 10^5$	2.22 ± 0.12	$99.37 \pm 0.17\%$
		<i>B. subtilis</i>	0	$(7.24 \pm 4.90) \times 10^9$	0	0
			312.5	$(3.25 \pm 2.33) \times 10^9$	0.41 ± 0.09	$60.49 \pm 7.91\%$
			625	$(7.75 \pm 5.54) \times 10^6$	3.40 ± 0.64	$99.92 \pm 0.05\%$

2.6. Live/Dead Spore Viability Assay

Figure 5 shows the untreated (control) spores were primarily green. Samples treated with 312.5 µg/mL TFDG indicated the spores were impaired, while 625 µg/mL TFDG-treated spores were mainly non-viable.

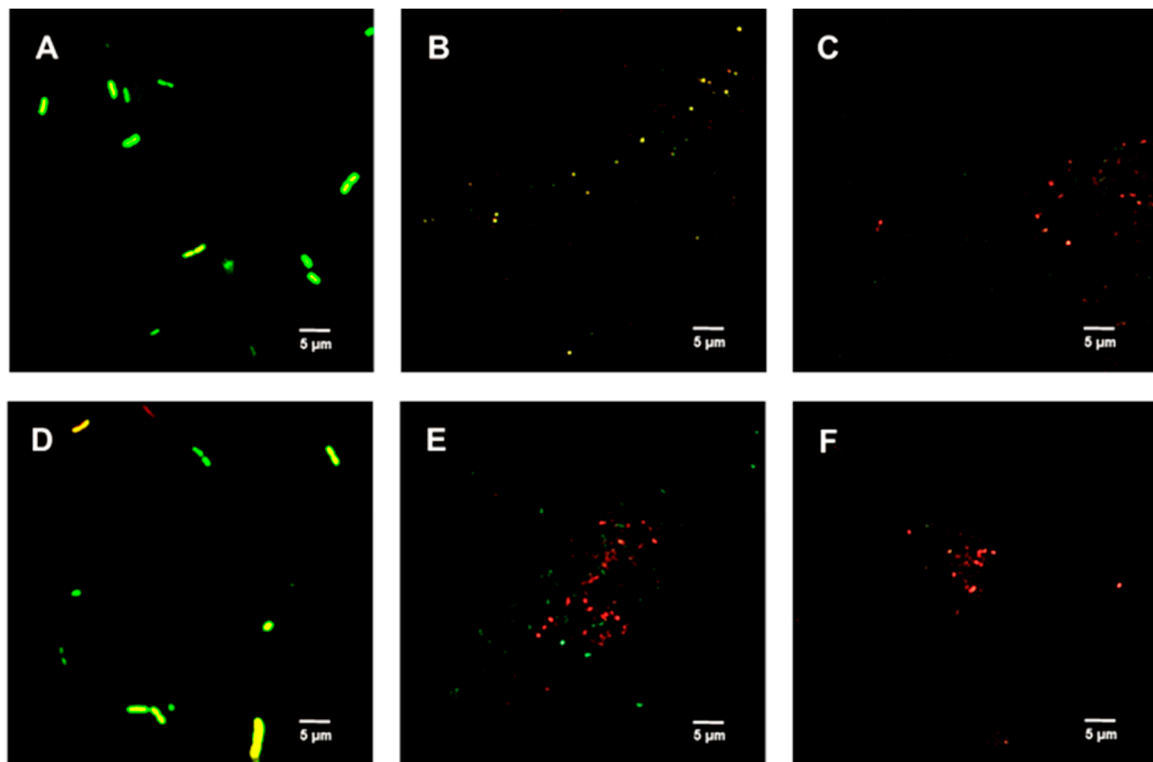


Figure 5. Live/Dead assay of *Bacillus* spp. spores with TFDG at 60-min incubation. The green indicates viable spores, while the red indicates non-viable spores. (A) *B. cereus* spores control; (B) *B. cereus* spores with 312.5 µg/mL TFDG; (C) *B. cereus* spores with 625 µg/mL TFDG; (D) *B. subtilis* spores control; (E) *B. subtilis* spores with 312.5 µg/mL TFDG; and (F) *B. subtilis* spores with 625 µg/mL TFDG.

2.7. Binding Pocket

The protein structures related to the four genes of interest were analyzed via CASTp to determine its binding pocket. Table 4 shows the binding pocket areas (\AA^2) for GPR were 616.45 and 433.40 for *B. cereus* and *B. subtilis*, respectively. The binding pocket areas (\AA^2) for Lgt were 1284.21 for *B. cereus* and 1565.20 for *B. subtilis*. The amino acid residues of each pocket were used as a guide to determine the location and size of the grid for *in silico* docking analysis.

Table 4. Binding pocket prediction and analysis of conserved germination protein via CASTp. The predicted binding pocket includes the pocket area, volume, and residues lining the pocket of conserved germination genes.

Bacteria	Protein	Pocket Area (Å ²)	Volume (Å ³)	Residue Lining Pocket
<i>B. cereus</i>	GPR	616.45	290.23	Arg196, Ser197, Ile198, Thr252, Ile253, Asp254, Phe255, Ile256, Leu257, Lys258, Phe260, Gly261, Arg262, Met264, Lys265, Ala304, Gly306, Glu309, Leu316, Leu319, Val320, Leu321, Ser322, Val330
	Lgt (GerF)	1284.21	1087.71	Trp3, Ile4, Val5, Arg6, Gln8, Pro9, Ser11, Leu12, Ile13, Gly15, Ser16, Gly19, Met23, Val41, Ala44, Phe45, Ile48, Ala49, Trp52, Lys53, Ile75, Lys79, His80, Val82, Cys85, Ile86, Ser89, Val90, Ile92, Leu107, Leu110, Pro111, Ile112, Ala113, Leu114, Cys115, Met116, Ser117, Ile118, Ile119, Phe120, Tyr 121, Glu154, Ala158, Leu159, Val162, Gly163, Leu165, Trp166, Ile178, Phe181, Leu182, Glu185, Gly186, His189, Phe203, Gly204, Met207, Gln208, Leu211, Ser212, Cys214, Val215, Leu218
<i>B. subtilis</i>	GPR	433.40	225.27	Arg44, His46, Lys50, Thr53, Asp55, Val56, Thr57, Glu59, Leu74, Ala76, Gln77, Gly78, Val90, Val93, Phe94, Glu96, Glu97, Ser99, Ala100, Phe101, Glu103, Asn104, Lys109, Ile206, Ile208, His355, Lys357, Val58, Ser359, Gln360, Asn362, Lys363, Gly364, Ser365, Tyr366, Asn367
	Lgt (GerF)	1565.20	1484.55	Leu18, Ala 19, His21, Tyr23, Gly24, Ile26, Ile27, Gly30, Ala31, Gly34, Ile37, Ala38, Arg40, Glu41, Lys44, Arg45, Gly46, Leu47, Phe52, Val56, Ala59, Ile60, Ala63, Ile64, Ala67, Ile89, Trp90, Gly93, Ile94, Gly99, Leu100, Ala103, Ile104, Thr106, Gly107, Leu116, Phe118, Lys120, Leu121, Ala122, Asp123, Ile124, Ala125, Ala126, Pro127, Ser128, Ile129, Leu 131, Gly132, Gln 133, Ile135, Gly136, Arg137, Gly139, Asn140, Glu145, Phe180, Glu183, Ser187, Ile192, Leu196, Arg198, Arg199, Ala200, Asn201, Leu202, Arg203, Arg204, Glu206, Met207, Phe208, Tyr211, Ile212, Tyr215, Arg219, Arg226, Thr233, Asp234, Ser235, Leu236

2.8. In Silico Docking Analysis

Table 5 details the molecular docking result of TFDG for both GPR and Lgt in *B. cereus* and *B. subtilis*. The *B. cereus* GPR docking score was -9.7 kcal/mol with five bonds, including conventional H-bond and Pi-Stacked. *B. cereus* Lgt binding score with TFDG was -7.6 kcal/mol with five different bonds that include conventional H-bond and pi-cation. Both GPR and Lgt of *B. subtilis* had the same binding score of -10.3 kcal/mol, but GPR has 12 bonds, including conventional H-bond, unfavorable donor-donor, and pi-donor H-bond. In contrast, Lgt has only seven bonds, including hydrophobic pi-sigma, conventional H bond, and carbon H bond. The binding pocket and the bond for each protein were observed using Discovery Studio, as seen in Figure 6.

Table 5. Docking analysis of conserved germination proteins. The molecular interaction of TFDG with various genes. The table shows the best binding probability.

Bacteria	Protein	Docking Score (kcal/mol)	Interacting Residue	Distance	Category
<i>B. cereus</i>	GPR	−9.7	Trp120	2.51	Conventional H-bond
			Trp120	3.98, 3.88	Pi-Pi Stacked
			Asn121	2.59	Conventional H-bond
			Val163	2.78	Conventional H-bond
			Glu340	2.37	Conventional H-bond
	Lgt (GerF)	−7.6	Lys26	1.85	Conventional H-bond
			Lys26	3.73	Pi-Cation
			Ser31	2.99	Conventional H-bond
			Lys168	2.00	Conventional H-bond
			Arg171	2.51	Conventional H-bond
<i>B. subtilis</i>	GPR	−10.3	Gly119	2.06, 2.94	Conventional H-bond
			ASN120	2.34	Conventional H-bond
			ASN120	2.92	Conventional H-bond
			ASN120	2.03	Conventional H-bond
			ASN120	1.97	Conventional H-bond
			ASN122	1.68	Unfavorable Donor-Donor
			ASP126	2.97	Conventional H-bond
			Ile170	1.93	Conventional H-bond
			Thr172	3.05	Pi Donor H-bond
	Lys222	1.22	Unfavorable Donor-Donor		
	Lgt (GerF)	−10.3	Ala63	3.78	Hydrophobic Pi-Sigma
			Ala103	3.62	Hydrophobic Pi-Sigma
			Ala103	2.07	Conventional H-Bond
			Ile129	3.29	Carbon Hydrogen Bond
			Gly132	3.96	Hydrophobic Pi-Sigma
Tyr215			1.92	Conventional H-bond	
Asp234	2.38	Conventional H-bond			

Previous studies showed the -7.0 kcal/mol threshold as significant for AutoDock binding [48,49]. Since both proteins showed a higher negative value, it indicates these two are good candidates for TFDG anti-germination properties evaluation. Hydrogen bond regulates molecular interaction through donor-acceptor pairing, enhancing receptor-ligand interaction [50]. Instead, hydrophobic interaction is a major consideration for binding affinity as this interaction can be considered a weak hydrogen bond [50]. *B. cereus* GPR binding affinity consists of 4 hydrogen bond interactions, while Lgt (GerF) consists of four hydrogen interactions. *B. subtilis* GPR TFDG binding affinity consists of nine hydrogen bonds interactions, while Lgt (GerF) has four hydrogen bonds and three strengthening hydrophobic interactions.

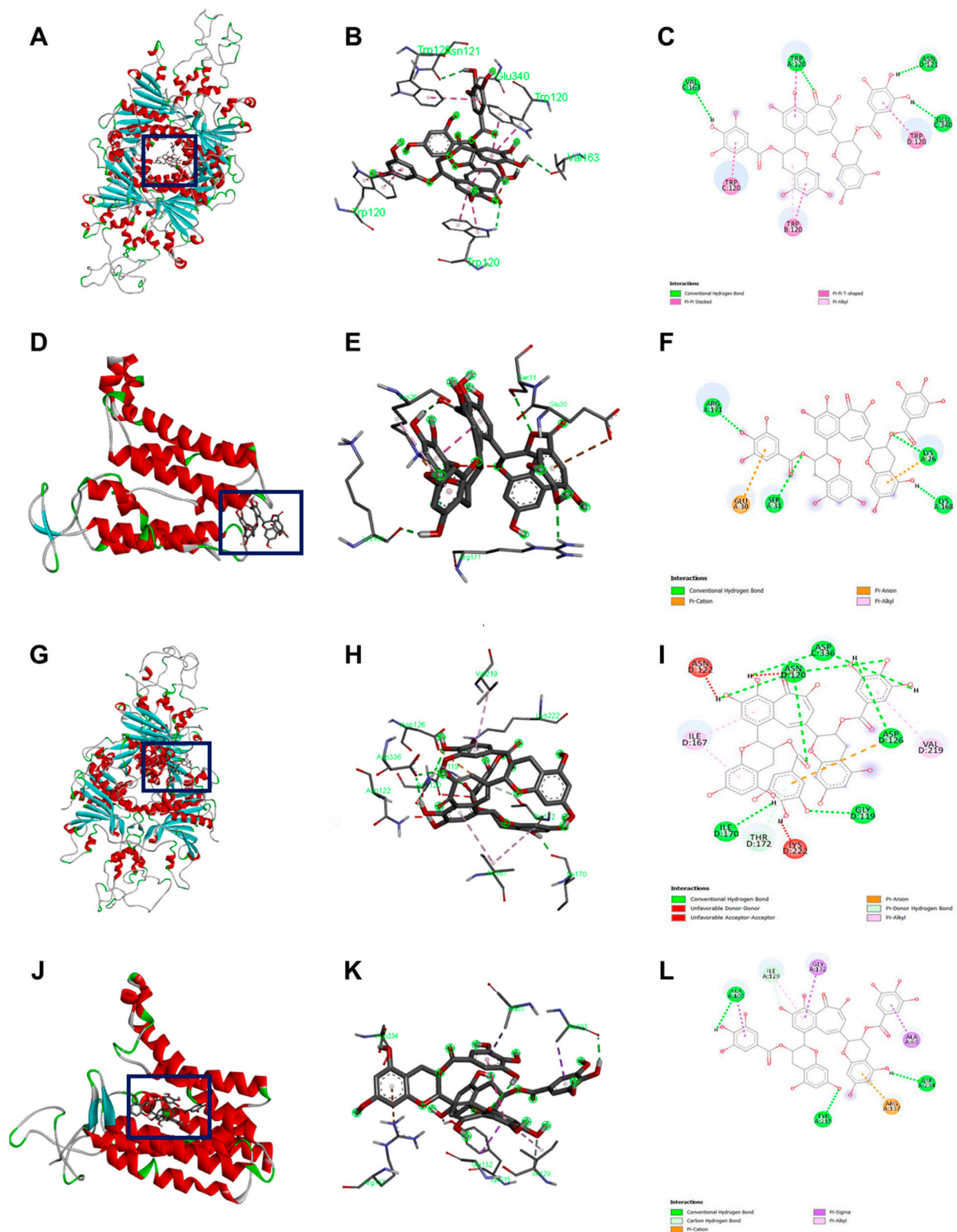


Figure 6. Docking visualization of TFDG with the germination protein using BIOVIA Discovery Studio Visualizer. (A–C) *B. cereus* GPR with TFDG; (D–F) *B. cereus* Lgt with TFDG; (G–I) *B. subtilis* GPR with TFDG; (J–L) *B. subtilis* Lgt with TFDG. For (C,F,I,L) the bright green line shows conventional hydrogen bond; bright pink shows the pi-pi interaction; light pink shows pi-alkyl interaction; orange shows pi cation, pi carbon, and pi-anion interaction; the red line shows unfavorable bond interaction; light green shows pi-donor hydrogen interaction and carbon-hydrogen interaction; and bright purple shows pi sigma interaction.

2.9. Semi-Quantitative RT-PCR

Figure 7 shows the relative expression of both *lgt* and *gpr* after a one-hour treatment of 625 µg/mL TFDG. In both *B. cereus* and *B. subtilis*, the expression of *gpr* dropped to 0.20 and 0.39, respectively, compared to the control (1.00). On the other hand, the expression of *lgt* was lower only in *B. cereus* (0.25) but not in *B. subtilis* (0.88) when compared to the control (1.00).

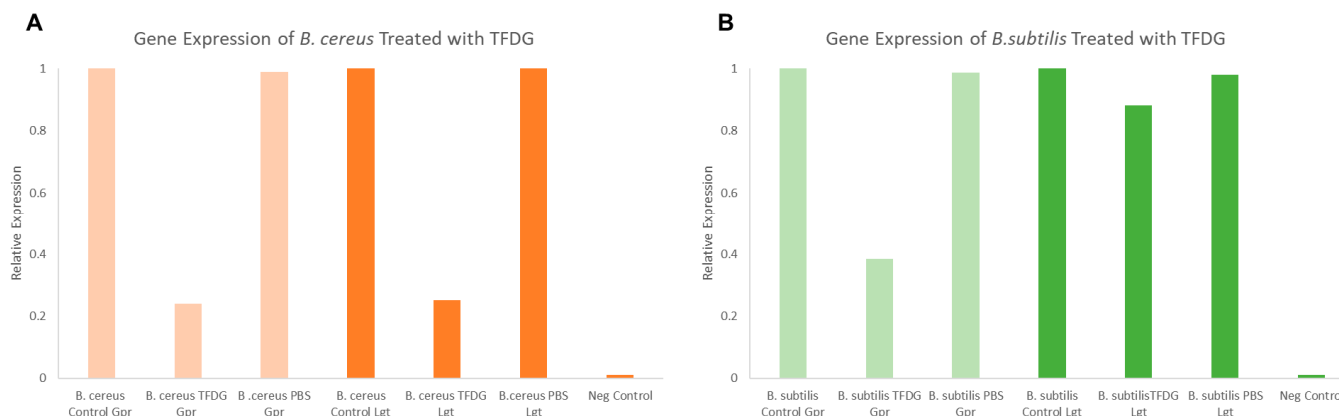


Figure 7. Semi-quantitative RT-PCR *lgt* and *gpr* gene expression analysis of *Bacillus* spore when treated with TFDG. (A) *B. cereus* spores; (B) *B. subtilis* spores.

3. Discussion

The urgency to find a novel antimicrobial agent has pushed researchers to look for either natural or synthetic alternatives. Currently, there are 42 new antibiotics under clinical development, but only 11 can treat pathogens that are considered critical by the World Health Organization (WHO) [51]. Antibiotic development projects from major pharmaceutical companies only account for four out of 42 studies, focusing on more profitable ventures like immune-oncology therapeutics [51]. For this reason, it is time for us to seek alternative solutions to ease the healthcare and economic burden of developing new antibiotics.

In this study, several methods were used to demonstrate the effectiveness of TFDG in inhibiting cell growth. As seen in Figures 2–4 and Tables 1 and 2, 250 µg/mL TFDG consistently inhibits $\geq 90\%$ of cells compared to the control at 6-h incubation. BacTiter-Glo™ measures the ATP level in the cell since extracellular ATP peaked at the end of the log phase but decreased during the stationary phase [52]. This test is more sensitive as it directly detects the presence of the ATP level in the sample, indicating the metabolically active viable cells, which do not discriminate between live and dead cells [53]. The Live/Dead assay measures the permeability of the cellular membrane. Red-colored cells indicate the cell membranes were damaged when treated with TFDG (Figures 2–4). These two assays provided further proof that TFDG could effectively inhibit bacterial growth. Ignasimuthu et al. [54] showed the MIC of EGCG for *B. subtilis*, *E. coli*, and *S. aureus* ranging from 130 to 580 µg/mL via broth dilution method. This suggests that TFDG might be comparable or even better as an antibacterial agent when compared to EGCG. Further studies of the effects of TFDG against clinically significant strains like ESKAPE (*Enterococcus faecium*, *S. aureus*, *K. pneumoniae*, *A. baumannii*, *P. aeruginosa*, and *Enterobacter* spp.) bacteria and other drug-resistant strains such as MRSA, VRSA, carbapenem-resistant Enterobacterales (CRE) will be carried out [55]. In terms of the antibacterial mechanism, TFDG decreased the eDNA and dextran production in *S. mutans* while decreasing the expression nucleoid synthesis in *Clostridium perfringens* (*C. perfringens*) [9,13]. A recent transcriptome study also shows that TFs (80% purity) could inhibit different virulence factors, including glucosyltransferases, *gtfB*, *gtfC*, and *gtfD* in *S. mutans*. The antimicrobial mechanism of TFDG on other species remains undetermined [56].

Bacterial spores are associated with foodborne diseases and food spoilage, and human diseases like gas gangrene, anthrax, and botulism [36]. Table 3 and Figure 5 show the successful inhibition of both *B. cereus* and *B. subtilis* from germinating. This is a promising observation, as TFDG could still prevent the spore from germinating above 99% for both species. The ability of EGCG to inhibit sporulation is well-documented across *Bacillus* spp. [16,57]. The findings in this study provide further evidence that tea polyphenols could serve as a potent antimicrobial agent. CASTp is an online tool that analytically predicts pocket cavities by utilizing the algorithmic and theoretical modeling that excludes shallow depression [58]. This binding pocket was utilized to determine the binding affinity of TFDG. Molecular docking in this study helps understand the mechanism of TFDG. Previous findings showed that compounds with binding energies of -7.0 kcal/mol or less are considered significant [48]. This threshold eliminates either weak or non-specific binding energies [49]. Chang et al. [49] showed that this threshold could detect 98% of known inhibitors of HIV therapeutics. This threshold has also been shown to eliminate 95% of non-inhibitor interaction [49]. This study uses AutoDock Vina for binding analysis. It is a freely accessible tool that best performed in predicting high-affinity ligands and showed the most consistent performance in a study by Kukol [59]. Table 4 and Figure 6 show that the binding affinity of TFDG for *B. cereus* GPR and Lgt were -9.7 and -7.6 kcal/mol, respectively. As for *B. subtilis*, TFDG affinity for GPR and Lgt were the same, at -10.3 kcal/mol. Based on the promising binding results, a semi-quantitative RT-PCR was carried out to investigate the relative expression of both genes when treated with TFDG. This method is sensitive and reliable in detecting limited transcripts from the samples [60]. The result in Figure 7 shows that the relative expression of *gpr* was significantly lower (0.20 to 0.39) than the control in both *B. cereus* and *B. subtilis*. The relative expression of *lgt* was higher in *B. subtilis* (0.88) than *B. cereus* (0.25) compared to the control. Overall, TFDG may affect both *lgt* and *gpr* expression in *B. cereus* while only *gpr* expression in *B. subtilis*. The GPR protease encoded by *gpr* is a germination protease in the spore coat, responsible for degrading the small acid-soluble protein (SASPs) [61]. This is a conserved gene in *Bacillus* spp. *Clostridium* spp. and *Clostridioides* spp. involving in protein synthesis and energy metabolism for early spore outgrowth [61,62]. A conserved gene, *lgt* or *gerF* in *Bacillus* spp. and *Clostridium* spp. codes for prelipoprotein diacylglycerol transferase [62,63]. This enzyme acts as a catalyst for the transfer of diacylglycerol to a cysteine residue in bacterial membrane prelipoproteins [63]. Mutation in this gene results in a slower germination process even in a favorable environment [63,64]. The deletion of *lgt* in *B. anthracis* causes a decrease in surface hydrophobicity that eventually leads to lower virulence in the mutant strain [64]. In *B. subtilis*, the mixture of Ca^{2+} and dipicolinic acid (Ca-DPA) complex with GerF occurs during germination [63]. Li et al. [65] reported that the binding dissociation constant (Kd) between Ca-DPA and its native ligand SpoVAD was 0.8. To the best of our knowledge, this is the first study that investigates the binding affinity between Ca-DPA and GerF in *Bacillus* spp. Both GPR and GerF show favorable outcomes in inhibiting the germination process from *in silico* analysis. The favorable binding affinity, along with multiple numbers of hydrogen and hydrophobic bonds, suggests that these two proteins could be the potential targets of TFDG in inhibiting the germination process. Semi-quantitative results support that TFDG inhibits the expression of the conserved genes. Thus, TFDG should be further investigated as a natural food additive.

Figures 2–4 show the cells clumped together, the self-binding process known as auto-agglutination/auto-aggregation [66]. This is a widely observed phenomenon and is considered the first step in biofilm formation [66]. Auto-aggregation occurs under stressful conditions, such as temperature change, and protects the cells from external stressors [66]. Generally, auto-aggregation is mediated by surface proteins like the self-associating autotransporters (SAATs) in *Enterobacteriaceae* [66]. In *Actinobacillus pleuropneumoniae* (*A. pleuropneumoniae*), the adhesin gene *adh* was involved in the biofilm formation, and the deletion of this gene could decrease pathogenicity [67]. Similarly, the first steps of biofilm formation in *Helicobacter pylori*, *P. gingivalis*, and *Staphylococcus epidermidis* are also through

auto-aggregation via their adhesin genes [68–70]. The effects of TFDG, especially pertaining to adhesion and biofilm formation, would be a pivotal step to better understanding the antimicrobial mechanism of TFDG.

4. Materials and Methods

4.1. Bacteria Culture

The bacterial cultures used in this study include Gram-negative: *Klebsiella aerogenes* (*K. aerogenes*) (155030A), *Escherichia coli* (*E. coli*) (155065A), *Pseudomonas aeruginosa* (*P. aeruginosa*) (155250A), and *Proteus mirabilis* (*P. mirabilis*) (155239A); Gram-positive: *Bacillus cereus* (*B. cereus*) (154870A), *Bacillus subtilis* (*B. subtilis*) (154921A), *Staphylococcus aureus* (*S. aureus*) (155554A), and *Streptococcus pyogenes* (*S. pyogenes*) (155630A); and acid-fast *Mycobacterium smegmatis* (*M. smegmatis*) (155180A). All cultures were obtained from Carolina Biological (Carolina Biological, Burlington, NC, USA).

4.2. Culture Maintenance

All cultures were maintained in tryptic soy broth (TSB) or tryptic soy agar (TSA) except for *S. pyogenes* and *M. smegmatis*, which were maintained in brain heart infusion broth (BHIB) (Bacto™, Sparks, MD, USA). The media were made with Milli-Q Integral 5 Water Purification System (Millipore Sigma, Billerica, MA, USA) based on the manufacturer's protocol. All experiments were performed using fresh overnight culture. The purity of the cultures was routinely checked.

4.3. Theaflavin Preparation

Theaflavins were obtained from a nutraceutical company (DH Nutraceuticals, LLC, Edison, NJ, USA). Theaflavin-3,3'-digallate (TFDG) was extracted and purified using ethyl acetate fraction, LH-20 column, 40% acetone solution elution then concentrated via rotary evaporator [71]. Purified 10 mg/mL TFDG stock solution was prepared with 200 proof ethanol (EtOH) (DLI, King of Prussia, PA, USA). The theaflavin stock was diluted in bacterial growth media to the desired concentrations accordingly.

4.4. Microplate Assay

The bacterial growth was monitored with different TFDG concentrations (0, 62.5, 125, and 250 µg/mL) over a 12-h period. In a 96-well plate, 10 µL of overnight culture ($OD_{600nm} = 1.0$) was added to each well along with various concentrations of TFDG and TSB to yield a final volume of 120 µL. The optical density was recorded hourly using a Varioskan™ LUX multimode microplate reader and analyzed via SkanIt Software (Thermo Scientific™, Waltham, MA, USA). The positive control was 10% bleach, while bacterial growth media was used as the negative control. The highest solvent concentration (1% EtOH) was also tested. Erythromycin, a broad-spectrum antibiotic, has also been included as a reference molecule for antibacterial efficacy comparison. The experiments were performed in triplicate. The microplate assay results established the half-maximal inhibitory concentration (IC_{50}) and minimum inhibitory concentration (MIC). The lowest concentration with no bacterial growth was defined as MIC. The IC_{50} was calculated based on a dose-response curve with log (concentration) as the x-axis and percent inhibition as the y-axis based on 0, 62.5, 125, and 250 µg/mL. The concentration that correlates to the 50% inhibition is the IC_{50} .

4.5. Colony Forming Unit (CFU) Assay

Following the microplate assay, the cultures treated with 0, 62.5, and 250 µg/mL TFDG were collected after 6-h incubation, serially diluted (from 10^{-2} to 10^{-8}) plated on TSA. The plates were incubated for 12 h at 37 °C, and the experiments were done in triplicate. The CFUs were recorded, and the percent inhibition was calculated based on the following formula:

$$\text{Percent Inhibition} = \left[\frac{CFU_{\text{untreated}} - CFU_{\text{treated}}}{CFU_{\text{untreated}}} \right] \times 100 \quad (1)$$

The log reduction of the CFU was also calculated based on the following formula:

$$\text{Log Reduction} = \text{Log}_{10} \left(\frac{\text{CFU}_{\text{untreated}}}{\text{CFU}_{\text{treated}}} \right) \quad (2)$$

4.6. BacTiter-Glo™ Microbial Cell Viability Assay

BacTiter-Glo™, the luciferase-based assay that quantifies the amount of ATP of metabolically active cells, was conducted according to the manufacturer's protocol (Promega, Madison, WI, USA) [54]. The reagent was prepared by mixing the BacTiter-Glo™ buffer with the BacTiter-Glo™ lyophilized substrate at room temperature. The mixture was then homogenized and incubated at room temperature for 15 min.

In a black 96-well plate, the bacteria were prepared based on the microplate assay (TFDG concentration of 0, 62.5, and 250 µg/mL) and placed in an IS-500 Incubator Shaker (Chemglass Life Sciences LLC, Vineland, NJ, USA) at 37 °C, 250 rpm for six hours. Then 120 µL of the BacTiter-Glo™ reagent was added to each well. The plate was wrapped in aluminum foil and placed in the incubator shaker for five minutes. The luminescence was read using a Varioskan™ LUX multimode microplate reader and analyzed via SkanIt Software (Thermo Scientific™, Waltham, MA, USA). The experiments were done in triplicate. The percent inhibition was calculated based on the following formula:

$$\text{Percent Inhibition} = \left[\frac{(\text{RFU}_{\text{untreated}} - \text{RFU}_{\text{treated}})}{\text{RFU}_{\text{untreated}}} \right] \times 100 \quad (3)$$

The log reduction of the RFU was also calculated based on the following formula:

$$\text{Log Reduction} = \text{Log}_{10} \left(\frac{\text{RFU}_{\text{untreated}}}{\text{RFU}_{\text{treated}}} \right) \quad (4)$$

4.7. LIVE/DEAD™ BacLight™ Bacterial Viability Assay

The Live/Dead Viability is a two-dye system consisting of Syto9 green fluorescent dye and propidium iodide (PI) red fluorescent dye. Both nucleic acid dyes can be used to differentiate live from dead bacteria. PI penetrates damaged bacterial membranes while Syto9 stains bacteria with intact cell membranes. Thus, live cells will be stained in green, impaired cells in yellow, and dead cells in red.

The staining was done using the Invitrogen™ Live/Dead BacLight™ Bacterial Viability Kit. According to the manufacturer's recommendation, equal parts of the Syto9 and PI were combined (Thermo Fisher Scientific, Waltham, MA, USA).

Following the same experimental setup as the CFU assay mentioned above (0, 62.5, and 250 µg/mL TFDG), the dye mixture was added to each culture and incubated at room temperature in the dark for 15 min. The cells were then observed using Olympus IX81 FV1000 Confocal Microscope, and the images were analyzed using the FV10-ASW 4.2 viewer. This method was also utilized to visualize the germinated spores, except the spores were treated for 60 min.

4.8. Spore Preparation

This method was modified based on the previously published protocol [16,72]. *B. cereus* and *B. subtilis* are spore-forming bacteria. The spores were induced by adding 5 mL of fresh overnight culture ($\text{OD}_{600\text{nm}} = 1.0$) to 5 mL sterile diH₂O in a culture tube. The cultures were incubated at 37 °C and 250 rpm for 72 h (IS-500 Incubator Shaker, Chemglass Life Sciences LLC, Vineland, NJ, USA). After 72 h, the spores were heated for 20 min at 75 °C to inactivate the vegetative cells. The purity of the spores was confirmed through the Schaeffer Fulton differential stain method.

4.9. Spore Germination Inhibition Assay

100 µL of the 72-h spores were added to various concentrations of TFDG (312.5 µg/mL and 625 µg/mL) along with TSB to a final volume of 1 mL in a microcentrifuge tube. The tubes were incubated for 1 h at 37 °C and 250 rpm (IS-500 Incubator Shaker, Chemglass Life Sciences LLC, Vineland, NJ, USA). After the incubation period, the samples were serially diluted (from 10⁻² to 10⁻⁹), and 100 µL of the dilution was plated using the spread plate method with TSA. The plates were incubated for 12 h at 37 °C. The experiments were done in triplicate. The CFUs were recorded, and the percentage of inhibition and log reduction was calculated based on the formula above (1 and 2).

4.10. Ligand Preparation

The 2D structure of TFDG (structure ID: 135403795) was obtained from PubChem (<https://pubchem.ncbi.nlm.nih.gov/>, accessed on 27 August 2021). The structure was converted into 3D format using Vega ZZ software (<http://www.vegazz.net>, accessed on 27 August 2021) and .pdbqt file format using AutoDock Tools V1.5.6 [73].

4.11. Gene and Protein Selection

The germination genes for *in silico* modeling were selected based on conserveness in *Bacillus* spp. and *Clostridium* spp. [74]. The genes and their protein information were tabulated in Table 6. The protein structure of each gene was downloaded directly from PDB (<https://www.rcsb.org/>, accessed on 3 September 2021) for the binding analysis. If the protein structure was not yet crystalized, the protein sequence was used to construct a hypothetical structure using SwissModel (<https://swissmodel.expasy.org/>, accessed on 3 September 2021) [75]. The hypothetical structure with the highest sequence identity was chosen for the analysis. The binding pocket was then determined using the Computed Atlas of Surface Topography of Proteins (CASTp) (<http://sts.bioe.uic.edu/castp/>, accessed on 3 September 2021) [58].

Table 6. Genes and protein information of conserved germination genes of *B. cereus* and *B. subtilis*.

Bacteria	Gene	NCBI Gene ID	Crystal Structure	PDB Reference	% Sequence Identity
<i>B. cereus</i>	<i>gpr</i>	56320307	None	IC8B	71.47%
	<i>lgt (gerF)</i>	56322894	None	5AZC	16.74%
<i>B. subtilis</i>	<i>gpr</i>	937838	None	IC8B	68.68%
	<i>lgt (gerF)</i>	12085459	None	5AZC	35.21%

4.12. In Silico Docking Analysis and Visualization

In silico docking analysis was performed using AutoDock Vina. The size and search space of each protein were calculated using AutoDock Tools 1.5.6 based on the result from the CASTp analysis. Table 7 shows the grid box for each analysis. The spacing was left at the default value of 0.375 Å, as well as the exhaustiveness rate of 8 [73].

Table 7. Grid box information of conserved germination protein for binding analysis.

Bacteria	Protein	Center X	Center Y	Center Z	Size X	Size Y	Size Z
<i>B. cereus</i>	GPR	-2	10	110	126	126	126
	Lgt (GerF)	-20	0	0	92	120	104
<i>B. subtilis</i>	GPR	-20	40	50	126	126	126
	Lgt (GerF)	-15	0	-8	90	114	126

4.13. Total RNA Extraction, cDNA Synthesis, and Semi-Quantitative RT-PCR

The spore germination assay was carried out for control, PBS, and 625 µg/mL TFDG. After one hour of treatment, the RNA extraction was done using the Ambion® RiboPure™ Kit (Ambion Inc, Austin, TX, USA). Then 250 µL of the sample was mixed with the 1 mL TRI reagent. The mixture was sonicated 15 times at 3 s intervals (20% power) using the Branson Sonifier Cell Disruptor 200 (Emerson Industrial, St. Louis, MO, USA). The extraction process was carried out based on the manufacturer's protocol. The RNA was used as a template for the cDNA synthesis using the ABI High Capacity cDNA Reverse Transcription Kit (Applied Biosystems-Life Technologies, Camarillo, CA, USA). The cDNA synthesis was done according to the manufacturer's protocol. The cDNA synthesis was carried out in a Veriti 96-Well Thermocycler (Applied Biosystems, Camarillo, CA, USA). The cDNA purity and concentration were measured using a BioDrop uLite (Biochrom, Cambridge, United Kingdom). The samples were stored at −20 °C.

The oligonucleotides were designed based using NCBI Primer Design Tool (<https://www.ncbi.nlm.nih.gov/tools/primer-blast/>, accessed 3 November 2021). The following primers were generated: Bc_GPR_F2: 5'-ACACCAGATGCTCTTGGACC-3' and Bc_GPR_R2: 5'-TCTGCTCTTTTCATCCGGCA-3'; Bc_Lgt_F2: 5'-CTGTATGGGCTTTTGGGGCA and Bc_Lgt_R2: 5'-TGAGCAAACCCCTCAACAAT-3'; Bs_GPR_F2: 5'-CCGATTTGGCAGTGGAAACG-3' and Bs_GPR_R2: 5'-AACACCAAGCGTGTCTTTGC-3'; Bs_Lgt_F2: 5'-TTTGCTCGGGCTGTGGATAG-3' and Bs_Lgt_R2 5' CCCTTGACGCGTCTGAAGAT-3'; 16S ribosomal RNA 27F: 5'-AGAGTTTGATCCTGGCTCAG-3' and 1492R: 5'-ACGGCTACCTTGTTACGACTT-3'. The ~100 µg/mL cDNA was used, and the PCR was performed using the Applied Biosystems Veriti 96-Well Thermal Cycler (ThermoFisher Scientific, MA, USA): 95 °C for 60 s, 35 cycles of 95 °C for 10 s, 56 °C for 10 s and 72 °C for 90 s. A 2% agarose gel electrophoresis was carried out, and the amount of cDNA was determined [76]. The relative mRNA expression was then calculated.

4.14. Statistical Analysis

All experiments were performed in triplicate, and the mean and standard deviations (SD) were calculated. One-way Analysis of Variance (ANOVA) and Dunnett's post hoc analysis were used to analyze the data (GraphPad Prism 5, San Diego, CA, USA). A *p*-value less than 0.05 was considered statistically significant.

5. Conclusions

This study profiled the effects of TFDG on nine bacteria, including Gram-positive, Gram-negative, and acid-fast bacteria. Microplate assay and the CFU assay were carried out. The microplate assay results indicated the MIC was 250 µg/mL. BacTiter-Glo™ Microbial Cell Viability test was also performed to measure the level of ATP in the sample. The fluorescence-based Live/Dead Assay was utilized to visualize the morphological changes on individual cells to TFDG, thus precluding the possible antibacterial mechanism of TFDG. *In silico* modeling allowed us to analyze and propose the mechanism of TFDG on the bacterial spores at the molecular level. Semi-quantitative RT-PCR assays were carried out for gene expression analysis pre- and post-treatment. This study successfully shows the potential usage of TFDG as an antimicrobial agent for a wide selection of bacteria, ranging through Gram-negative, Gram-positive, and acid-fast species. This study also shows the anti-germination properties of TFDG as TFDG inhibits the expression of *gpr* and *lgt*, genes code for the conserved GPR and Lgt (GerF) germination proteins based on *in silico* modeling and semi-quantitative RT-PCR.

Supplementary Materials: The following supporting information can be downloaded at: <https://www.mdpi.com/article/10.3390/ijms23042153/s1>.

Author Contributions: Conceptualization, A.Y. and T.C.; methodology, A.Y. and T.C.; investigation, A.Y., B.C., O.F. and S.L.; formal analysis, A.Y. and T.C.; resources, T.C.; data curation, A.Y.; writing—original draft preparation, A.Y.; writing—review and editing, T.C.; visualization, A.Y. and T.C.;

supervision, T.C.; project administration, T.C.; funding acquisition, T.C. All authors have read and agreed to the published version of the manuscript.

Funding: A.Y. and S.L. were supported by the Seton Hall University (SHU) Graduate Teaching Assistantship. TC is supported by the SHU Biological Sciences Research Fund and the William and Doreen Wong Foundation.

Data Availability Statement: Data are contained within the article.

Conflicts of Interest: The authors declare no conflict of interest.

References

- Piddock, L.J.V. The crisis of no new antibiotics—What is the way forward? *Lancet Infect. Dis.* **2012**, *12*, 249–253. [[CrossRef](#)]
- Ventola, C.L. The Antibiotic Resistance Crisis Part 1: Causes and Threats. *Pharm. Ther.* **2015**, *40*, 277–283.
- CDC. *Antibiotic Resistance Threats in the United States*; US Department of Health and Human Services, CDC: Atlanta, GA, USA, 2019. [[CrossRef](#)]
- Martens, E.; Demain, A.L. The antibiotic resistance crisis, with a focus on the United States. *J. Antibiot.* **2017**, *70*, 520–526. [[CrossRef](#)]
- Hilal, Y.; Engelhardt, U. Characterisation of white tea—Comparison to green and black tea. *J. Verbrauch. Lebensm.* **2007**, *2*, 414–421. [[CrossRef](#)]
- Babich, H.; Gottesman, R.T.; Liebling, E.J.; Schuck, A.G. Theaflavin-3-gallate and theaflavin-3'-gallate, polyphenols in black tea with prooxidant properties. *Basic Clin. Pharmacol. Toxicol.* **2008**, *103*, 66–74. [[CrossRef](#)] [[PubMed](#)]
- Pereira-Caro, G.; Moreno-Rojas, J.M.; Brindani, N.; Del Rio, D.; Lean, M.E.J.; Hara, Y.; Crozier, A. Bioavailability of Black Tea Theaflavins: Absorption, Metabolism, and Colonic Catabolism. *J. Agric. Food Chem.* **2017**, *65*, 5365–5374. [[CrossRef](#)] [[PubMed](#)]
- de Oliveira, A.; Prince, D.; Lo, C.Y.; Lee, L.H.; Chu, T.C. Antiviral activity of theaflavin digallate against herpes simplex virus type 1. *Antivir. Res.* **2015**, *118*, 56–67. [[CrossRef](#)]
- Wang, S.; Wang, Y.; Wang, Y.; Duan, Z.; Ling, Z.; Wu, W.; Tong, S.; Wang, H.; Deng, S. Theaflavin-3,3'-Digallate Suppresses Biofilm Formation, Acid Production, and Acid Tolerance in *Streptococcus mutans* by Targeting Virulence Factors. *Front. Microbiol.* **2019**, *10*, 1705. [[CrossRef](#)]
- Engelhardt, U.H. Chemistry of Tea. In *Comprehensive Natural Products II*; Elsevier Science: Amsterdam, The Netherlands, 2010; pp. 999–1032.
- Peterson, J.; Dwyer, J.; Jacques, P.; Rand, W.; Prior, R.; Chui, K. Tea variety and brewing techniques influence flavonoid content of black tea. *J. Food Compos. Anal.* **2004**, *17*, 397–405. [[CrossRef](#)]
- Leung, L.K.; Su, Y.; Chen, R.; Zhang, Z.; Huang, Y.; Chen, Z.-Y. Theaflavins in Black Tea and Catechins in Green Tea Are Equally Effective Antioxidants. *J. Nutr.* **2001**, *131*, 2248–2251. [[CrossRef](#)]
- Noor Mohammadi, T.; Maung, A.T.; Sato, J.; Sonoda, T.; Masuda, Y.; Honjoh, K.; Miyamoto, T. Mechanism for antibacterial action of epigallocatechin gallate and theaflavin-3,3'-digallate on *Clostridium perfringens*. *J. Appl. Microbiol.* **2019**, *126*, 633–640. [[CrossRef](#)] [[PubMed](#)]
- Hui, X.; Yue, Q.; Zhang, D.D.; Li, H.; Yang, S.Q.; Gao, W.Y. Antimicrobial mechanism of theaflavins: They target 1-deoxy-D-xylulose 5-phosphate reductoisomerase, the key enzyme of the MEP terpenoid biosynthetic pathway. *Sci. Rep.* **2016**, *6*, 38945. [[CrossRef](#)] [[PubMed](#)]
- Teng, Z.; Guo, Y.; Liu, X.; Zhang, J.; Niu, X.; Yu, Q.; Deng, X.; Wang, J. Theaflavin-3,3-digallate increases the antibacterial activity of β -lactam antibiotics by inhibiting metallo-beta-lactamase activity. *J. Cell Mol. Med.* **2019**, *23*, 6955–6964. [[CrossRef](#)] [[PubMed](#)]
- Ali, B.; Lee, L.H.; Laskar, N.; Shaikh, N.; Tahir, H.; Hsu, S.D.; Newby, R., Jr.; Valsechi-Diaz, J.; Chu, T. Modified Green Tea Polyphenols, EGCG-S and LTP, Inhibit Endospore in Three *Bacillus* spp. *Adv. Microbiol.* **2017**, *7*, 175–187. [[CrossRef](#)]
- Renzetti, A.; Betts, J.W.; Fukumoto, K.; Rutherford, R.N. Antibacterial green tea catechins from a molecular perspective: Mechanisms of action and structure-activity relationships. *Food Funct.* **2020**, *11*, 9370–9396. [[CrossRef](#)]
- Ben Lagha, A.; Grenier, D. Black tea theaflavins attenuate *Porphyromonas gingivalis* virulence properties, modulate gingival keratinocyte tight junction integrity and exert anti-inflammatory activity. *J. Periodontol. Res.* **2017**, *52*, 458–470. [[CrossRef](#)]
- Chowdhury, P.; Sahuc, M.E.; Rouille, Y.; Riviere, C.; Bonneau, N.; Vandeputte, A.; Brodin, P.; Goswami, M.; Bandyopadhyay, T.; Dubuisson, J.; et al. Theaflavins, polyphenols of black tea, inhibit entry of hepatitis C virus in cell culture. *PLoS ONE* **2018**, *13*, e0198226. [[CrossRef](#)]
- Kong, J.; Zhang, G.; Xia, K.; Diao, C.; Yang, X.; Zuo, X.; Li, Y.; Liang, X. Tooth brushing using toothpaste containing theaflavins reduces the oral pathogenic bacteria in healthy adults. *3 Biotech* **2021**, *11*, 150. [[CrossRef](#)]
- Wang, M.; Li, J.; Hu, T.; Zhao, H. Metabolic fate of tea polyphenols and their crosstalk with gut microbiota. *Food Sci. Hum. Wellness* **2022**, *11*, 455–466. [[CrossRef](#)]
- Passarelli-Araujo, H.; Palmeiro, J.K.; Moharana, K.C.; Pedrosa-Silva, F.; Dalla-Costa, L.M.; Venancio, T.M. Genomic analysis unveils important aspects of population structure, virulence, and antimicrobial resistance in *Klebsiella aerogenes*. *FEBS J.* **2019**, *286*, 3797–3810. [[CrossRef](#)]
- Kaper, J.B.; Nataro, J.P.; Mobley, H.L. Pathogenic *Escherichia coli*. *Nat. Rev. Microbiol.* **2004**, *2*, 123–140. [[CrossRef](#)] [[PubMed](#)]

24. Sondi, I.; Salopek-Sondi, B. Silver nanoparticles as antimicrobial agent: A case study on *E. coli* as a model for Gram-negative bacteria. *J. Colloid Interface Sci.* **2004**, *275*, 177–182. [[CrossRef](#)] [[PubMed](#)]
25. Blount, Z.D. The Natural History of Model Organisms: The unexhausted potential of *E. coli*. *elife* **2015**, *4*, e05826. [[CrossRef](#)] [[PubMed](#)]
26. Iakovides, I.C.; Michael-Kordatou, I.; Moreira, N.F.F.; Ribeiro, A.R.; Fernandes, T.; Pereira, M.F.R.; Nunes, O.C.; Manaia, C.M.; Silva, A.M.T.; Fatta-Kassinos, D. Continuous ozonation of urban wastewater: Removal of antibiotics, antibiotic-resistant *Escherichia coli* and antibiotic resistance genes and phytotoxicity. *Water Res.* **2019**, *159*, 333–347. [[CrossRef](#)] [[PubMed](#)]
27. Zhang, C.M.; Xu, L.M.; Wang, X.C.; Zhuang, K.; Liu, Q.Q. Effects of ultraviolet disinfection on antibiotic-resistant *Escherichia coli* from wastewater: Inactivation, antibiotic resistance profiles and antibiotic resistance genes. *J. Appl. Microbiol.* **2017**, *123*, 295–306. [[CrossRef](#)] [[PubMed](#)]
28. Roth, N.; Kasbohrer, A.; Mayrhofer, S.; Zitz, U.; Hofacre, C.; Domig, K.J. The application of antibiotics in broiler production and the resulting antibiotic resistance in *Escherichia coli*: A global overview. *Poult. Sci.* **2019**, *98*, 1791–1804. [[CrossRef](#)]
29. Davis, G.S.; Waits, K.; Nordstrom, L.; Grande, H.; Weaver, B.; Papp, K.; Horwinski, J.; Koch, B.; Hungate, B.A.; Liu, C.M.; et al. Antibiotic-resistant *Escherichia coli* from retail poultry meat with different antibiotic use claims. *BMC Microbiol.* **2018**, *18*, 174. [[CrossRef](#)]
30. Poole, K. *Pseudomonas aeruginosa*: Resistance to the max. *Front. Microbiol.* **2011**, *2*, 65. [[CrossRef](#)]
31. Hamilton, A.L.; Kamm, M.A.; Ng, S.C.; Morrison, M. *Proteus* spp. as Putative Gastrointestinal Pathogens. *Clin. Microbiol. Rev.* **2018**, *31*, e00085-17. [[CrossRef](#)]
32. Cohen-Nahum, K.; Sidel-Odes, L.; Riesenber, K.; Schlaeffer, F.; Borer, A. Urinary tract infections caused by multi-drug resistant *Proteus mirabilis*: Risk factors and clinical outcomes. *Infection* **2010**, *38*, 41–46. [[CrossRef](#)]
33. Ehling-Schulz, M.; Lereclus, D.; Koehler, T.M. The *Bacillus cereus* Group: *Bacillus* Species with Pathogenic Potential. *Microbiol. Spectr.* **2019**, *7*. [[CrossRef](#)] [[PubMed](#)]
34. Errington, J.; Aart, L.T.V. Microbe Profile: *Bacillus subtilis*: Model organism for cellular development, and industrial workhorse. *Microbiology* **2020**, *166*, 425–427. [[CrossRef](#)] [[PubMed](#)]
35. Pogmore, A.R.; Seistrup, K.H.; Strahl, H. The Gram-positive model organism *Bacillus subtilis* does not form microscopically detectable cardiolipin-specific lipid domains. *Microbiology* **2018**, *164*, 475–482. [[CrossRef](#)] [[PubMed](#)]
36. Setlow, P. Germination of Spores of *Bacillus* Species: What We Know and Do Not Know. *J. Bacteriol.* **2014**, *196*, 1297–1305. [[CrossRef](#)]
37. Keijsers, B.J.; Ter Beek, A.; Rauwerda, H.; Schuren, F.; Montijn, R.; van der Spek, H.; Brul, S. Analysis of temporal gene expression during *Bacillus subtilis* spore germination and outgrowth. *J. Bacteriol.* **2007**, *189*, 3624–3634. [[CrossRef](#)]
38. Levinson, H.S.; Hyatt, M. Effects of Temperature on Activation, Germination, and Outgrowth of *Bacillus megaterium* Spores. *J. Bacteriol.* **1970**, *101*, 56–64. [[CrossRef](#)]
39. Hornstra, L.M.; de Vries, Y.P.; Wells-Bennik, M.H.; de Vos, W.M.; Abee, T. Characterization of germination receptors of *Bacillus cereus* ATCC 14579. *Appl. Environ. Microbiol.* **2006**, *72*, 44–53. [[CrossRef](#)]
40. Traag, B.A.; Pugliese, A.; Eisen, J.A.; Losick, R. Gene Conservation among Endospore-Forming Bacteria Reveals Additional Sporulation Genes in *Bacillus subtilis*. *J. Bacteriol.* **2013**, *195*, 253–260. [[CrossRef](#)]
41. Seo, Y.S.; Lee, D.Y.; Rayamahji, N.; Kang, M.L.; Yoo, H.S. Biofilm-forming associated genotypic and phenotypic characteristics of *Staphylococcus* spp. isolated from animals and air. *Res. Vet. Sci.* **2008**, *85*, 433–438. [[CrossRef](#)]
42. Sriskandan, S.; Faulkner, L.; Hopkins, P. *Streptococcus pyogenes*: Insight into the function of the streptococcal superantigens. *Int. J. Biochem. Cell Biol.* **2007**, *39*, 12–19. [[CrossRef](#)]
43. Zhu, L.; Olsen, R.J.; Horstmann, N.; Shelburne, S.A.; Fan, J.; Hu, Y.; Musser, J.M. Intergenic Variable-Number Tandem-Repeat Polymorphism Upstream of *rocA* Alters Toxin Production and Enhances Virulence in *Streptococcus pyogenes*. *Infect. Immun.* **2016**, *84*, 2086–2093. [[CrossRef](#)] [[PubMed](#)]
44. Forbes, B.A. Mycobacterial Taxonomy. *J. Clin. Microbiol.* **2017**, *55*, 380–383. [[CrossRef](#)] [[PubMed](#)]
45. WHO. *W.H.O. Global Tuberculosis Report*; World Health Organization: Geneva, Switzerland, 2020; pp. 1–232.
46. Lelovic, N.; Mitachi, K.; Yang, J.; Lemieux, M.R.; Ji, Y.; Kurosu, M. Application of *Mycobacterium smegmatis* as a surrogate to evaluate drug leads against *Mycobacterium tuberculosis*. *J. Antibiot.* **2020**, *73*, 780–789. [[CrossRef](#)] [[PubMed](#)]
47. Altaf, M.; Miller, C.H.; Bellows, D.S.; O’Toole, R. Evaluation of the *Mycobacterium smegmatis* and BCG models for the discovery of *Mycobacterium tuberculosis* inhibitors. *Tuberculosis* **2010**, *90*, 333–337. [[CrossRef](#)]
48. Kwofie, S.K.; Broni, E.; Asiedu, S.O.; Kwarko, G.B.; Dankwa, B.; Enniful, K.S.; Tiburu, E.K.; Wilson, M.D. Cheminformatics-Based Identification of Potential Novel Anti-SARS-CoV-2 Natural Compounds of African Origin. *Molecules* **2021**, *26*, 406. [[CrossRef](#)]
49. Chang, M.W.; Lindstrom, W.; Olson, A.J.; Belew, R.K. Analysis of HIV Wild-Type and Mutant Structures via in Silico Docking against Diverse Ligand Libraries. *J. Chem. Inf. Model.* **2007**, *47*, 1258–1262. [[CrossRef](#)]
50. Chen, D.; Oezguen, N.; Urvil, P.; Ferguson, C.; Dann, S.M.; Savidge, T.C. Regulation of protein-ligand binding affinity by hydrogen bond pairing. *Sci. Adv.* **2016**, *2*, e1501240. [[CrossRef](#)]
51. Ardal, C.; Balasegaram, M.; Laxminarayan, R.; McAdams, D.; Outtersson, K.; Rex, J.H.; Sumpradit, N. Antibiotic development—Economic, regulatory and societal challenges. *Nat. Rev. Microbiol.* **2020**, *18*, 267–274. [[CrossRef](#)]
52. Mempin, R.; Tran, H.; Chen, C.; Gong, H.; Kim Ho, K.; Lu, S. Release of extracellular ATP by bacteria during growth. *BMC Microbiol.* **2013**, *13*, 301. [[CrossRef](#)]

53. Reyneke, B.; Dobrowsky, P.H.; Ndlovu, T.; Khan, S.; Khan, W. EMA-qPCR to monitor the efficiency of a closed-coupled solar pasteurization system in reducing *Legionella* contamination of roof-harvested rainwater. *Sci. Total Environ.* **2016**, *553*, 662–670. [[CrossRef](#)]
54. Ignasimuthu, K.; Prakash, R.; Murthy, P.S.; Subban, N. Enhanced bioaccessibility of green tea polyphenols and lipophilic activity of EGCG octaacetate on gram-negative bacteria. *LWT* **2019**, *105*, 103–109. [[CrossRef](#)]
55. Santajit, S.; Indrawattana, N. Mechanisms of Antimicrobial Resistance in ESKAPE Pathogens. *Biomed. Res. Int.* **2016**, *2016*, 2475067. [[CrossRef](#)]
56. Feng, S.; Eucker, T.P.; Holly, M.K.; Konkel, M.E.; Lu, X.; Wang, S. Investigating the responses of *Cronobacter sakazakii* to garlic-derived organosulfur compounds: A systematic study of pathogenic-bacterium injury by use of high-throughput whole-transcriptome sequencing and confocal micro-Raman spectroscopy. *Appl. Environ. Microbiol.* **2014**, *80*, 959–971. [[CrossRef](#)]
57. Shigemune, N.; Nakayama, M.; Tsugukuni, T.; Hitomi, J.; Yoshizawa, C.; Mekada, Y.; Kurahachi, M.; Miyamoto, T. The mechanisms and effect of epigallocatechin gallate (EGCG) on the germination and proliferation of bacterial spores. *Food Control* **2012**, *27*, 269–274. [[CrossRef](#)]
58. Tian, W.; Chen, C.; Lei, X.; Zhao, J.; Liang, J. CASTp 3.0: Computed atlas of surface topography of proteins. *Nucleic Acids Res.* **2018**, *46*, W363–W367. [[CrossRef](#)] [[PubMed](#)]
59. Kukul, A. Consensus virtual screening approaches to predict protein ligands. *Eur. J. Med. Chem.* **2011**, *46*, 4661–4664. [[CrossRef](#)] [[PubMed](#)]
60. Marone, M.; Mozzetti, S.; Ritis, D.D.; Pierelli, L.; Scambia, G. Semiquantitative RT-PCR analysis to assess the expression levels of multiple transcripts from the same sample. *Biol. Proced. Online* **2001**, *3*, 19–25. [[CrossRef](#)] [[PubMed](#)]
61. Xiao, Y.; Francke, C.; Abee, T.; Wells-Bennik, M.H. Clostridial spore germination versus bacilli: Genome mining and current insights. *Food Microbiol.* **2011**, *28*, 266–274. [[CrossRef](#)]
62. Norsigian, C.J.; Danhof, H.A.; Brand, C.K.; Oezguen, N.; Midani, F.S.; Palsson, B.O.; Savidge, T.C.; Britton, R.A.; Spinler, J.K.; Monk, J.M. Systems biology analysis of the *Clostridioides difficile* core-genome contextualizes microenvironmental evolutionary pressures leading to genotypic and phenotypic divergence. *NPJ Syst. Biol. Appl.* **2020**, *6*, 31. [[CrossRef](#)]
63. Igarashi, T.; Setlow, B.; Paidhungat, M.; Setlow, P. Effects of a *gerF* (*lgt*) mutation on the germination of spores of *Bacillus subtilis*. *J. Bacteriol.* **2004**, *186*, 2984–2991. [[CrossRef](#)]
64. Okugawa, S.; Moayeri, M.; Pomerantsev, A.P.; Sastalla, I.; Crown, D.; Gupta, P.K.; Leppla, S.H. Lipoprotein biosynthesis by prolipoprotein diacylglyceryl transferase is required for efficient spore germination and full virulence of *Bacillus anthracis*. *Mol. Microbiol.* **2012**, *83*, 96–109. [[CrossRef](#)] [[PubMed](#)]
65. Li, Y.; Davis, A.; Korza, G.; Zhang, P.; Li, Y.Q.; Setlow, B.; Setlow, P.; Hao, B. Role of a SpoVA protein in dipicolinic acid uptake into developing spores of *Bacillus subtilis*. *J. Bacteriol.* **2012**, *194*, 1875–1884. [[CrossRef](#)] [[PubMed](#)]
66. Trunk, T.; Khalil, H.S.; Leo, J.C. Bacterial autoaggregation. *AIMS Microbiol.* **2018**, *4*, 140–164. [[CrossRef](#)]
67. Wang, L.; Qin, W.; Yang, S.; Zhai, R.; Zhou, L.; Sun, C.; Pan, F.; Ji, Q.; Wang, Y.; Gu, J.; et al. The Adh adhesin domain is required for trimeric autotransporter Apa1-mediated *Actinobacillus pleuropneumoniae* adhesion, autoaggregation, biofilm formation and pathogenicity. *Vet. Microbiol.* **2015**, *177*, 175–183. [[CrossRef](#)]
68. Yonezawa, H.; Osaki, T.; Kurata, S.; Zaman, C.; Hanawa, T.; Kamiya, S. Assessment of in vitro biofilm formation by *Helicobacter pylori*. *J. Gastroenterol. Hepatol.* **2010**, *25* (Suppl. 1), S90–S94. [[CrossRef](#)]
69. Yamaguchi, M.; Sato, K.; Yukitake, H.; Noiri, Y.; Ebisu, S.; Nakayama, K. A *Porphyromonas gingivalis* mutant defective in a putative glycosyltransferase exhibits defective biosynthesis of the polysaccharide portions of lipopolysaccharide, decreased gingipain activities, strong autoaggregation, and increased biofilm formation. *Infect. Immun.* **2010**, *78*, 3801–3812. [[CrossRef](#)] [[PubMed](#)]
70. Ziebuhr, W.; Heilmann, C.; Götz, F.; Meyer, P.; Wilms, K.; Straube, E.; Hacker, J. Detection of the intercellular adhesion gene cluster (*ica*) and phase variation in *Staphylococcus epidermidis* blood culture strains and mucosal isolates. *Infect. Immun.* **1997**, *65*, 890–896. [[CrossRef](#)]
71. Lo, C.Y.; Li, S.; Tan, D.; Pan, M.H.; Sang, S.; Ho, C.T. Trapping reactions of reactive carbonyl species with tea polyphenols in simulated physiological conditions. *Mol. Nutr. Food Res.* **2006**, *50*, 1118–1128. [[CrossRef](#)]
72. Gray, D.A.; Dugar, G.; Gamba, P.; Strahl, H.; Jonker, M.J.; Hamoen, L.W. Extreme slow growth as alternative strategy to survive deep starvation in bacteria. *Nat. Commun.* **2019**, *10*, 890. [[CrossRef](#)]
73. Trott, O.; Olson, A.J. AutoDock Vina: Improving the speed and accuracy of docking with a new scoring function, efficient optimization, and multithreading. *J. Comput. Chem.* **2010**, *31*, 455–461. [[CrossRef](#)]
74. Galperin, M.Y.; Mekhedov, S.L.; Puigbo, P.; Smirnov, S.; Wolf, Y.I.; Rigden, D.J. Genomic determinants of sporulation in *Bacilli* and *Clostridia*: Towards the minimal set of sporulation-specific genes. *Environ. Microbiol.* **2012**, *14*, 2870–2890. [[CrossRef](#)] [[PubMed](#)]
75. Waterhouse, A.; Bertoni, M.; Bienert, S.; Studer, G.; Tauriello, G.; Gumienny, R.; Heer, F.T.; de Beer, T.A.P.; Rempfer, C.; Bordoli, L.; et al. SWISS-MODEL: Homology modelling of protein structures and complexes. *Nucleic Acids Res.* **2018**, *46*, W296–W303. [[CrossRef](#)] [[PubMed](#)]
76. Alambra, J.R.; Alenton, R.R.R.; Gulpeo, P.C.R.; Mecnas, C.L.; Miranda, A.P.; Thomas, R.C.; Velando, M.K.S.; Vitug, L.D.; Maningas, M.B.B. Immunomodulatory effects of turmeric, *Curcuma longa* (Magnoliophyta, Zingiberaceae) on *Macrobrachium rosenbergii* (Crustacea, Palaemonidae) against *Vibrio alginolyticus* (Proteobacteria, Vibrionaceae). *Aquac. Aquar. Conserv. Legis. Int. J. Bioflux Soc.* **2012**, *5*, 13–17.